

Kelly C. Smith\*

Matthew D. Eastin

Department of Geography and Earth Sciences,  
University of North Carolina at Charlotte, Charlotte, NC

## 1. INTRODUCTION

Tropical cyclones intensify through a combination of processes, including environmental interactions, heat and moisture exchanges with the oceans, and inner-core dynamical processes. Environmental factors known to favor TC intensification include: warm sea-surface temperatures (SSTs), minimal deep-layer vertical wind shear, high mid-tropospheric relative humidity, large low-level relative vorticity, and enhanced upper-level eddy angular momentum flux convergence (Kaplan and DeMaria 2003). Oceans provide the required heat and moisture to sustain the TC's deep convection, upper-level warm core, and intense surface winds. This energy is transferred from the ocean via surface fluxes. Greater fluxes, which favor TC intensification, occur when a storm passes over deep, warm ocean features such as warm-core eddies, loop currents, and the Gulf Stream (Shay et al. 2000; Hong et al. 2000). Finally, internal symmetric and asymmetric dynamical processes can lead to intensification. Such processes are linked to mesoscale convective features, including mesovortices, vortex Rossby waves (VRWs), deep convective hot towers (HTs), vortical hot towers (VHTs), and eyewall replacement cycles (Eastin et al. 2005b; Simpson et al. 1998; Hendricks et al. 2004; Montgomery and Kallenbach 1997; Willoughby 1990; many others). This research will focus on the implications of one particular component of internal dynamics, the VHT.

Before discussing the role of VHTs to intensification, a brief review of the HT route to intensification is warranted. HTs are tall cumulonimbus towers containing undilute or nearly undilute updrafts that transport high equivalent potential temperature ( $\Theta_e$ ) air from the subcloud layer to the upper troposphere, reaching or penetrating the tropopause (Simpson et al. 1998). Even though the intrinsic scale of HTs has not been formally defined in previous literature, the term has historically referred to towers with approximately 5 km wide updrafts (e.g. Riehl and Malkus 1958; Malkus

et al. 1961; Simpson et al. 1998). The general idea behind the HT is that deep convective cells in the TC eyewall lead to maintenance or intensification of the parent vortex by localized latent heat release in the eyewall at upper levels of the troposphere. A local overturning circulation, similar to the one mentioned in Shapiro and Willoughby (1982), produces local (i.e. asymmetric) descent within the eye, leading to adiabatic warming. The collective heating of the warm core lowers the pressure in the eye, thus increasing the pressure gradient, which in turn, increases the tangential winds. Multiple HTs can amplify this process.

Although HT theory helps explain aspects of intensification/RI, a combination of the VRW and HT concepts may provide new insights into the dynamics behind RI. Hendricks et al. (2004; hereafter HMD04) proposed a new mechanism for tropical cyclogenesis that involved a hot tower that rotated as it ascended, and introduced the term "vortical hot tower" to distinguish it from the classic hot tower of Riehl and Malkus (1958). VHTs are loosely defined as cores of deep cumulonimbus convection possessing strong vertical vorticity, arising from buoyancy-induced convergence, tilting, and stretching of local vorticity in a vorticity-rich environment (HMD04). VHTs differ from the deep, vertically penetrating convection of the HT in that the tilting and stretching of elevated pre-existing vorticity by intense convection yields a strong rotational component of the tower (Reasor et al. 2005). The horizontal scale of VHTs is on the order of 10 km in diameter, yet at finer scales the diameter was 5 to 7 km, and for an actual TC, Hurricane Dolly (1996) had VHT diameters on the order of 10-20 km. Peak core vertical velocity ranged from  $8.8 \text{ m s}^{-1}$  to  $15 \text{ m s}^{-1}$ , while the peak diabatic heating rate was  $150 \text{ K h}^{-1}$  at midlevels of the troposphere ( $z = 5 \text{ km}$ ). VHTs typically last approximately 1 h, but some have been seen for as much as 3 h in models. They are formed in two stages according to HMD04 and Van Sang et al. (2007). The first stage is preconditioning of the local environment via diabatic production of multiple small-scale, lower-tropospheric, cyclonic PV anomalies. Through tilting and stretching of the ambient vorticity environment, there is ample vorticity to be used for the second stage, merger and axisymmetrization of the convectively-generated PV anomalies. For the

---

\*Corresponding Author Address: Kelly C. Smith, Department of Geography and Earth Sciences, University of North Carolina at Charlotte, 9201 University City Blvd, Charlotte, NC 28223; email: kellsmit@uncc.edu

purposes of the current study, the first stage, vertical vorticity preconditioning, is inconsequential due to this study's focus on mature hurricanes, which already possess ample ambient vorticity.

As a caveat, the concept of VHTs was first developed to explain the transition of a mid-level cyclonic vortex to a surface cyclone; therefore, the following functions of VHTs are biased towards the genesis stage, and may or may not apply to VHTs in mature hurricanes. The role of the VHT goes beyond that of the HT. VHTs lead to intensity and structural change of the TC through quick convective events, as opposed to slow axisymmetric intensification (Van Sang et al. 2008). Their net effect is to produce strong, small scale (10 km diameter on average), lower-tropospheric (below  $z = 2.5$  km) cyclonic PV towers. The strong updrafts converge and stretch existing low-level vertical vorticity into intense small-scale vortex tubes. These tubes merge (usually at the surface first (Montgomery et al. 2006)) and axisymmetrize forming tubes that possess more vorticity than before axisymmetrization. The vorticity aspect, as compared to HTs in general, is expected to inhibit lateral entrainment (i.e. Julien et al. 1996) by effectively trapping the latent heat associated with the VHT and protecting the heat energy from being disbursed to the environment via gravity waves, thereby making VHT convection more efficient (HMD04). This efficient, nearly undiluted convection helps form/bolster the warm core, leading to intensification as previously discussed. Also, tangential momentum is increased due to the net influx of low-level angular momentum, as proposed by VRW theory (HMD04).

Other recent studies have begun to expand on the seminal VHT works of HMD04 and Montgomery et al. (2006). Numerical simulations of VHTs include Sippel et al. (2006), Van Sang et al. (2008), and Rogers 2009. In addition, there have been several observational studies by Reasor et al. (2005), Hendricks and Montgomery (2006), Molinari and Vollaro (2008; 2009), and Houze et al. (2009). It should be noted that all of these studies concentrated on cyclogenesis, whereas the current study focuses on VHTs in a mature hurricane.

The purpose of this study is to provide a better understanding of the kinematic processes related to rapid intensification by examining the mass flux characteristics, occurrence frequency, structural characteristics, and proximity to other mesoscale and convective-scale features of VHTs in a mature hurricane. It is not the intent of this study to formally explain the role of VHTs with respect to other inner-core processes, or to suggest that VHTs alone are the primary mechanism for RI. As previously stated, intensification is a combination of inner-core, environmental, and oceanic processes. No one of these

can be isolated in an observational study. Other methods, such as idealized and full physics numerical simulations, would need to be utilized to determine the specific role and impact of VHTs in RI.

## 2. DATA AND METHODS

Hurricane Guillermo (1997) was observed by two NOAA WP-3D research aircraft (N42RF and N43RF) on 2 August between 1830 UTC and 0030 UTC 3 August. Both aircraft were equipped with a 5.5 cm wavelength lower fuselage (LF) radar and a 3.2 cm wavelength tail Doppler radar (Jorgensen 1984) that were used to collect hydrometeor reflectivity and, in the case of the Doppler radar, velocity measurements. Each aircraft completed passes through Guillermo's inner core in order to obtain a dual-Doppler evaluation of the eye and eyewall wind fields. N42RF made 10 passes (20 radial legs) at  $\sim 3$ -km altitude while N43RF made 6 passes (12 radial legs) at  $\sim 5.5$ -km altitude. The tail radar on N42RF scanned in the track-normal plane while N43RF's tail radar scanned in the fore/aft scanning technique (FAST) mode (Gamache et al. 1995). The time between each pass averaged  $\sim 34$  min. For evaluation of the three-dimensional wind field, the Doppler radar analysis method of Gamache (1997) was employed. A Doppler-derived total wind field was decomposed following methodology by Reasor et al. (2000).

## 3. CLASSIFICATION OF INTENSE UPDRAFTS

Since, HTs and VHTs are representative of anomalously intense updrafts, convective cores with such traits were sought in the dataset. Updrafts with extremely high vertical velocity, or extreme updrafts (XUPs), were separated from non-extreme updrafts, heretofore called ordinary updrafts (ORDs), broadly based on the 90<sup>th</sup> percentile of all hurricane eyewall updrafts (Black et al. 1996). For this study, the various classes of updrafts are based on XUPs in Guillermo and further differentiated by height of the updraft and vorticity characteristics of the XUP. Criteria were established in order to easily differentiate between these traits.

The vertical velocity and vertical vorticity components analyzed utilized perturbation values (i.e., azimuthal wavenumbers greater than or equal to one) rather than total values of the components. This was done so as to isolate the asymmetric circulations from the symmetric dynamics. In other words, the same characteristics of VHTs in two storms could be compared using the same definition, whether or not the storms possess equivalent intensities, environments, or evolutionary characteristics.

For this study, unique criteria were developed to define XUPs based on their depth and vortical nature, since there are no standard definitions for these entities. XUPs are defined as cores of positive (upward) vertical motion within and inclusive of a  $+5 \text{ m s}^{-1}$  perturbation vertical velocity contour with a depth of at least 1 km (or two vertical grid points). XUPs were then differentiated by the vertical extent of the  $+5 \text{ m s}^{-1}$  perturbation vertical velocity contour. Shallow extreme updrafts (SEUs) are XUPs that have a depth of  $<6 \text{ km}$ . Conversely, deep extreme updrafts (DEUs) are XUPs that have a depth  $\geq 6 \text{ km}$ , loosely following the definitions by Riehl and Malkus (1958), Simpson et al. (1998), and Kelley and Stout (2004). DEUs are further separated by a perturbation vorticity threshold and height requirement. VHTs are DEUs with a strong cyclonic component around their vertical axes. VHTs follow the same definition of DEUs with two additional constraints. First, the deep updraft must be collocated with a positive perturbation vertical vorticity contour  $\geq 1 \times 10^{-3} \text{ s}^{-1}$  through no less than half of the depth of the hot tower. Second, the positive perturbation vertical vorticity maximum must be at the same height as or below the maximum of positive perturbation vertical velocity for the updraft. Conversely, HTs are DEUs that do not meet the vorticity thresholds of VHTs. See Fig. 1 for a hierarchical depiction of updraft classifications used in this study.

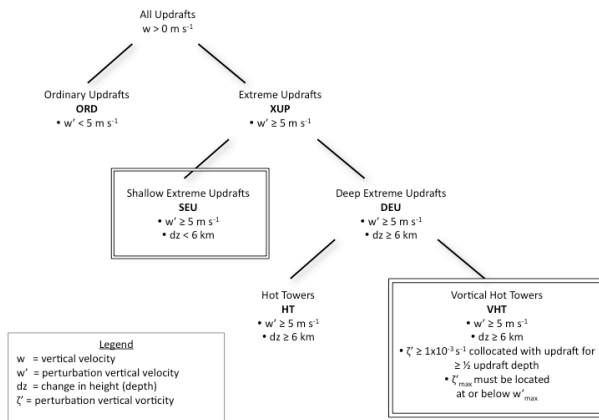


**Figure 1: Hierarchical representation of updrafts in tropical cyclones. Each branch to the right adds further constraints to the definition above it. Acronyms, along with constraints are listed below each term.**

#### 4. METHODOLOGY

For this study two primary methods for evaluating the characteristics of updrafts were utilized: a collection of census information and an evaluation of composite structures. This study compares and contrasts VHTs and SEUs through the examination of various census

and composited information. It is the focus of this investigation to elucidate the similarities and differences of VHTs, representing the deep and highly vortical updrafts, and SEUs, represented by updrafts that, as will be shown, represent a more common form of XUPs.

#### Census Methodology

Both methods relied on the previously mentioned azimuthally decomposed three-dimensional dual-Doppler radar data. The updrafts were found by initially locating the perturbation at each level (azimuthal wavenumbers  $\geq 1$ ) vertical velocity maxima for each updraft and the evaluating nearby grid points until the minimum threshold of  $5 \text{ m s}^{-1}$  was obtained. This demarked the edge of the updraft per the definition developed in Section 3 for XUPs. Census information collected included characteristics on the frequency, size, location, and mass flux of each identified XUP/SEU/DEU/HT/VHT.

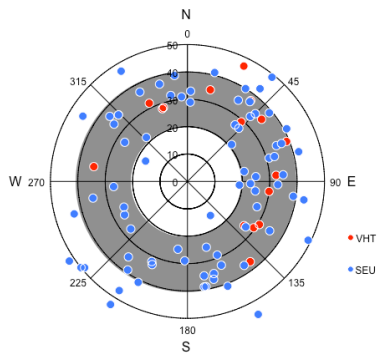
#### Composite Methodology

Compositing was performed to analyze the characteristics of nominal SEUs and VHTs in Hurricane Guillermo. Each updraft was segregated by type and moved both radially and azimuthally to a common location based upon the location of its perturbation vertical velocity maximum. In other words, all data within  $\pm 14 \text{ km}$  radially and  $\pm 90^\circ$  azimuthally of the updraft maximum were repositioned to a common grid centered on the updraft maximum. Azimuthal shifts were performed to serve as a central location for each updraft type, and to elucidate common structures and flow features located within  $\pm 45^\circ$  of the updraft centers. Radial shifts were performed in order to concentrate any common features within  $\pm 7 \text{ km}$  and to prevent radial skewing of the updraft features. The values at each corresponding three-dimensional grid point were then averaged based upon the number of updraft types analyzed.

## 5. RESULTS AND DISCUSSION

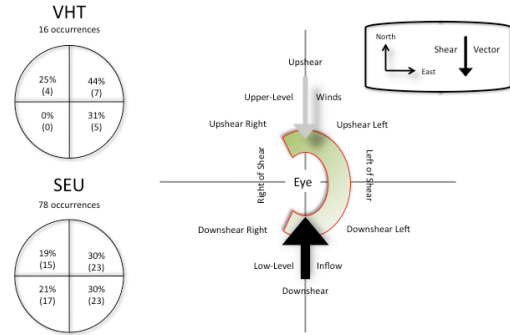
#### Census Results

Figure 2 shows an azimuthal-radial projection of all XUPs within a 60-km radius of the circulation center stratified into VHTs (red dots) and SEUs (blue dots). These particular locations are considered the center of the updraft when viewed from the top down, although the actual updraft may traverse much greater distances both azimuthally and radially when viewed in three dimensions. The locations of the XUPs as a whole do not appear to have a discernable pattern, with only slightly more located in the eastern semicircle (63 updrafts, or 61%) as compared to the western semicircle (39, or 39%).



**Figure 2: Azimuthal and radial locations of the positive vertical velocity maxima for vortical hot towers (VHT) and shallow extreme updrafts (SEU) for all aircraft passes through Guillermo on 2 August 1997. The azimuthal values are in units of degrees and the radial values are in km.**

Analyzing the updrafts stratified by the previously developed definitions for SEUs and VHTs and with respect to the environmental vertical shear allowed for patterns to be elucidated. Figure 3 provides the distributions of SEUs and VHTs with respect to the environmental shear vector. The shear vector was steady from the NNW during the study period. It is evident the VHTs are concentrated in the left-of-shear semicircle. While SEUs are observed in slightly greater numbers in the left-of-shear semicircle (60% of SEUs; 46), the distribution of VHTs is heavily weighted toward the left-of-shear semicircle (75% of VHTs; or 12 updrafts). Of the four VHTs located in the upshear-right quadrant, three of these existed within  $15^\circ$  of  $0^\circ$  (or due North); thus locating them slightly outside of the left-of-shear semicircle. In addition, radial distributions of VHTs and SEUs demonstrate the relative confinement of VHTs to the eyewall. 6% of VHTs (or 1 updraft) were observed with an updraft center location lying outside of a 40-km radius, and no VHTs were observed within 25 km of the center of circulation. In contrast, all shear quadrants are represented in the SEU distribution, with the two left-of-shear quadrants containing an equal number (or 31 updrafts, each). The two right-of-shear quadrants contained an almost equal number of SEUs, with the downshear-right quadrant and the upshear-right quadrant containing 20% and 19% of the updrafts, respectively. Also,  $\sim 26\%$  of SEUs (or 20 updrafts) were located outside of a 40-km radius along with  $\sim 6\%$  of SEUs (or 3 SEUs) existing inside of 20-km. Therefore, VHTs are far more concentrated within the eyewall than SEUs during this observation period of Guillermo.



**Figure 3: Azimuthal distributions of updraft classifications [shallow extreme updrafts (SEU) and vortical hot towers (VHT)] delineated into quadrants with respect to the environmental vertical wind shear vector (bold arrow, top right). Percentages are based on the number of occurrences in each quadrant (number in parentheses) as part of the total number of occurrences (listed above the circles). Various adjoining quadrants can be combined to form shear-relative semicircles to elucidate further relationships between updraft distributions.**

Coupling these VHT and SEU distributions with a persistent wavenumber-one reflectivity feature observed during all 10 radial passes, some initial conclusions can be made about the distribution differences between VHTs and SEUs. It can be surmised that VHTs are phenomena located primarily in the left-of-shear eyewall that are influenced greatly by asymmetric convection induced by the environmental vertical wind shear. In contrast, the distribution of SEUs may be influenced by the same mechanisms, but their more symmetric distribution and less radial concentration point to symmetric or other processes playing additional roles.

Figure 4 shows the depth of VHTs and SEUs as a function of azimuth. In addition to depth of each cells, the altitude of  $w'_{\max}$  for each of the updrafts is displayed with a hash mark. However, there appears to be an upward trend in the azimuthal distribution of cell depth in SEUs (Fig. 4 bottom) in the upshear-left quadrant and a downward trend in the right-of-shear semicircle. Comparative quadrant analyses using a two-tailed Student's t-test confirm the existence of a significant difference between the upshear-right quadrant and both the downshear-right and downshear-left quadrants (0.01 level), and to a lesser extent between the two upshear quadrants (0.05 level). In other words, the descending trend observed in the upshear-right quadrant is not observed in the downshear semicircle, and there exists a significant change in the upward trend of the upshear-left quadrant near due

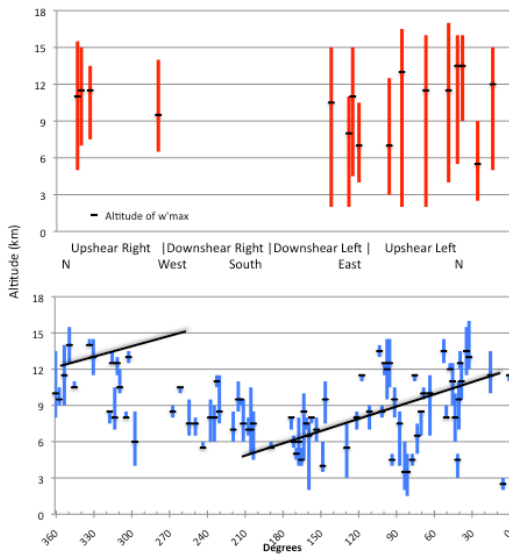


**Figure 4:** Azimuthal distributions of (top) vortical hot towers (VHT) and (bottom) shallow extreme updrafts (SEU) combined with vertical depth of each updraft (length of vertical bar). The altitude of the updraft maximum is denoted with a black hash. Minor tick marks on the vertical axis represent 0.5 km and 5 degrees on the horizontal axis. Vertical bars with multiple hash marks represent more than one updraft at that azimuth. Examining the plots from left to right provides a cyclonic scan of the updraft distributions.

North. The upshear-right quadrant may be a location of mature updrafts that have rotated cyclonically around the storm, inline with findings by Heymsfield et al. (2001). These updrafts could be dissipating DEUs that no longer meet the depth requirements to be classified as a DEU. This quadrant differs from the downshear semicircle in terms of updraft maturity; the downshear quadrants are a source region for updrafts when the storm is experiencing moderate vertical wind shear (Black et al. 2002). Therefore, the updrafts in this region are lower in the troposphere, and presumably are newer updrafts than the higher SEUs observed in the upshear quadrants.

In addition to the previously discussed azimuthal, radial, and vertical distributions of VHTs and SEUs, summary statistics were computed as a function of altitude. Vertical height level profiles were constructed per the methodology in Section 4. Table 1 lists the number of occurrences of each XUP classification per level, along with the subsequent percentage of the total number of possible updrafts for each updraft classification. All VHTs during the study period of Guillermo passed through the 9.0-km level, while only 25% were observed at the 2.0-km level. The largest occurrence of SEUs was observed at the 8.0-km level,

where 42% were observed. Therefore, each level will be more influenced by fewer updrafts for VHTs than for SEUs. The characteristics of any one updraft may bias each of the components to a greater extent for VHTs than for SEUs at a given height level.

Figure 5 demonstrates the vertical velocity profiles of VHTs and SEUs between the 2 and 16-km levels. This graph shows the significant differences in vertical velocity between the two updraft types. The mean maxima  $w$  values are  $10.65 \text{ m s}^{-1}$  at 11.5 km and  $8.25 \text{ m s}^{-1}$  at 10.0 km for VHTs and SEUs, respectively. Although there are significantly more SEUs than VHTs, the contribution of VHTs toward  $w$  is significant, especially in mid-to-upper levels.

**Table 1:** Percentage of Mass Flux (MF) for all rising motion compared to percentage of updraft area for each updraft type [extreme updrafts (XUP), shallow extreme updrafts (SEU), vortical hot towers (VHT), hot towers (HT), and deep extreme updrafts (DEU)].

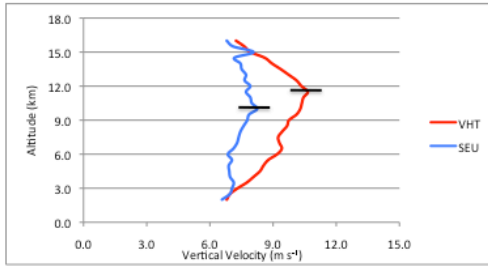
Updraft Type	3-km Altitude			6-km Altitude		
	Percentage of MF vs. All Rising Motion MF	Percentage of Updraft Area	MF/Area Ratio	Percentage of MF vs. All Rising Motion MF	Percentage of Updraft Area	MF/Area Ratio
XUP	5.57%	0.98%	5.67	16.61%	3.27%	5.08
SEU	1.78%	0.32%	5.62	4.32%	0.93%	4.62
DEU	3.79%	0.66%	5.70	12.29%	2.34%	5.26
HT	0.81%	0.16%	5.17	3.79%	0.78%	4.87
VHT	2.98%	0.51%	5.87	8.50%	1.56%	5.45

Updraft Type	9-km Altitude			12-km Altitude		
	Percentage of MF vs. All Rising Motion MF	Percentage of Updraft Area	MF/Area Ratio	Percentage of MF vs. All Rising Motion MF	Percentage of Updraft Area	MF/Area Ratio
	20.45%	4.32%	4.73	20.74%	4.00%	5.18
	4.13%	0.95%	4.37	5.07%	1.05%	4.83
	16.32%	3.38%	4.83	15.66%	2.95%	5.31
	3.87%	0.88%	4.41	1.26%	0.31%	4.04
	12.44%	2.50%	4.98	14.41%	2.64%	5.46

The depictions of vertical vorticity in Fig. 6 demonstrate the relative difference in vertical locations of strong vorticity between VHTs and SEUs. HMD04 found the vertical vorticity maximum of genesis VHTs to be at the 4-km level. This cell had a  $\zeta_{\text{tot}}$  value of  $7.2 \text{ s}^{-1}$ , while only extending from the 1.5 to 5-km levels. Since mesovortices are shallow, highly vortical updrafts generally existing within the eye-eyewall interface, it is possible that this anomalously high vorticity value is the result of this phenomenon. It should also be noted that the maximum vorticity value of 1.83 is located at the 9.0-km level. This location being lower than the maximum  $w'$  level of 11.5 is due to the definition of a VHT requiring that the  $\zeta'$  must be located at a level no higher than that of  $w'$  for each VHT updraft.

Although the definition by HMD04 stated that a VHT should be non-circular when sliced horizontally, an illustration of the significant differences in updraft size can be made by calculating an effective diameter. Using the total area inside the  $5 \text{ m s}^{-1}$   $w'$  contour, the effective diameter of this area, assuming circular geometry, was calculated at each level. Figure 7 shows the mean effective diameter for each updraft type as a



**Figure 5: Total average vertical velocity at each altitude for vortical hot towers (VHT) and shallow extreme updrafts (SEU). Black hash marks denote maxima.**

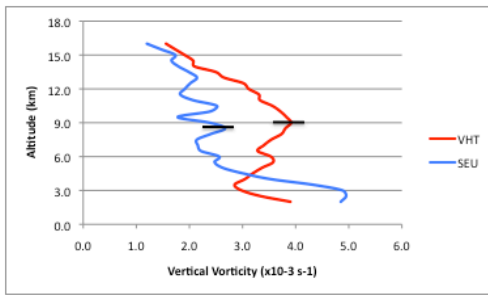


**Figure 6: Total average vertical vorticity at each altitude.**

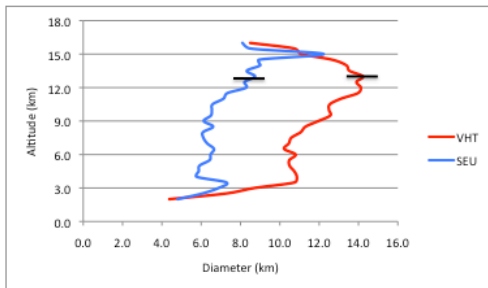


**Figure 7: Average updraft diameter at each altitude, delineated by the  $5 \text{ m s}^{-1}$  perturbation vertical velocity contour.**

function of height. Immediately it is apparent VHTs are substantially larger in diameter than their SEU counterparts. The median diameter for VHTs is 11.06 km, whereas the corresponding value for SEUs is 6.60

km. Therefore, VHTs have a 68% larger diameter than do the typical SEU. This results in a VHT updraft that occupies an area that is  $>2.5$  times larger than anominal SEU. The resultant difference in size will be the most substantial difference in mass transport to upper levels by the different classifications of updrafts. Also, these findings are in agreement with HMD04, Reasor et al. (2004), and Montgomery et al. (2006) which state that, for cyclogenesis, VHTs are features that have a diameter of  $\sim 10$  km.

Cumulative quantities of MF were examined to elucidate the contribution of each updraft type to the total mass transport of the storm. Initially, 5 levels (3, 6, 9, 12, and 15-km levels) were studied. Table 1 shows the component mass fluxes,  $MF_{tot}$ , the corresponding number of data points (occurrences) at each level, percentage of MF contribution of the updraft type, total area and percentage of updraft area at that level, and a MF/area percentage ratio. In each level studied, VHTs had a greater percentage of both MF and area as compared to SEUs. The greatest difference of the levels studied was the 9-km level. That was a unique level because all of the VHTs passed through that level. The VHTs were not necessarily fluxing their maximum amount of mass at that level; nevertheless, all of the VHTs were represented. At that height, VHTs occupied 2.6 times more area and fluxed 3.0 times more total mass than that of SEUs. Of the levels studied, both VHTs and SEUs attained their highest percentage of  $MF_{tot}$  at the 12-km level where they each fluxed 14.4% and 5.1% of the total mass, respectively. These percentages are further enhanced by the fact that each represented only 2.6% and 1.1% of the total updraft area, respectively. For VHTs, occupying such a small percentage of the total updraft area while fluxing  $\sim 15\%$  of the total mass demonstrates their significant contribution to the maintenance and deepening of the parent storm. While SEUs were represented by more than double the number of updrafts than VHTs, the VHTs fluxed 69% more total mass and occupied 50% more area than did the SEUs. SEUs, however, did attain their highest percentage of MF at this level with 6%. It is evident that as a portion of the total mass being transported from the surface to upper level, VHTs flux as much as 3 times the amount of mass while having 5 times fewer number of updrafts than that of SEUs. It is also noteworthy that VHTs transport as much as  $\sim 15\%$  of the mass in the storm but represent  $<2\%$  of all eyewall updrafts in observed TCs.

As previously mentioned, a ratio of the percentage of MF to the percentage of updraft area was computed at each of the study levels (Table 1). This ratio was computed to compare the relative contributions of each updraft class to one another. It was hypothesized that VHTs would contribute a far greater percentage of MF while occupying a far smaller percentage of the total

updraft area. Also, hypothesized was that the VHTs would have fluxed a much larger amount of mass per unit area than that of SEUs because the vortical nature of VHTs was hypothesized to prevent dry-air entrainment, thus providing a more undilute ascent of the air mass from lower levels to upper levels of the troposphere. In believing this, VHTs should have contributed more MF per area than did other updraft types, and thus would be a primary contributor to the total MF of the storm. A comparison of VHT and SEU MF/area percentage ratio showed these hypotheses were unsupported. The mean ratio for VHTs over the five study levels was 5.6 while the ratio was 5.1 for SEUs. These values suggest that the amount of mass fluxed was more than 5 times the area occupied by that type of updraft. The results calculated, however, suggest that VHTs provide a small increase in MF contribution per unit area (~10%) than do SEUs. This surprisingly small increase between the two updraft types is due to the difference in updraft velocities. The difference in updraft velocities has the potential to elucidate whether the vorticality of VHTs allows for a more unimpeded ascent, but without three-dimensional thermodynamic data, this hypothesis cannot be studied observationally.

### Composite Results

Three-dimensional composites were constructed to elucidate common structural and kinematic features in the vicinity of VHTs and SEUs. Little information was gleaned from composites of SEUs, since there were few commonalities between each updraft of that type. Substantial information was realized from the analysis of the VHT composite. Such information included the mean structure of the updraft and associated vertical vorticity core, as well as common locations of low-level mesovortices, convergent/divergent wind patterns, and adjacent updrafts/downrafts. The extraordinary features of VHTs will be the focus of the following discussion.

Figure 8 shows azimuthal-radial (top-down) plan views of the VHT composites depicting contours of perturbation vertical velocity (updraft; solid red lines), perturbation vertical vorticity (cyclonic vorticity; solid blue lines), radar reflectivity (gray shading), and perturbation wind vectors (black arrows) for azimuthal wavenumbers greater than two. This information is shown at cross sections at 10.5 km height, 0 km radially, and 0° azimuthally. These locations represent the horizontal location of composition and maximum  $\zeta$  of the composited VHT.

At the 6-km level (not shown) and above, airflow from upwind and inward of the VHT continues as the upper-levels of the eye-eyewall mesovortex are reached. There is noticeable cyclonic flow around the updraft as the vertical vorticity anomaly has become

more enhanced. As expected, there is a significant increase in the vertical wind velocities. A mid-to-upper level positive vorticity anomaly is first observed at this level extending from the innermost radii to center of the updraft while continuing through the depth of the VHT. The vorticity feature connects the lowest levels with the highest levels of the VHT. This prominent cyclonic motion is located downwind of the VHT at inner radii and midlevels, and extends to a region upwind of VHT center at upper levels. The vertical vorticity maximum ( $0.75 < \text{maximum} < 1.0 \text{ s}^{-1}$ ) is observed near 10.5 km altitude (Fig. 9) and -8 km radially. The maximum extends radially to +2 km and is bound vertically by

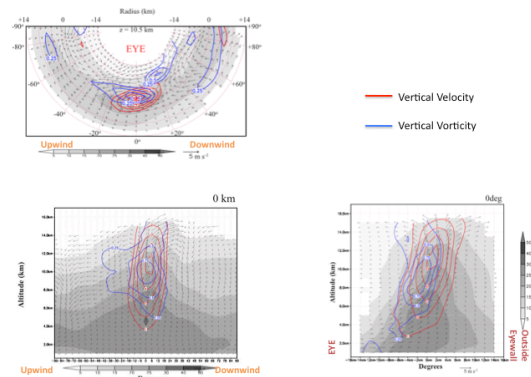


**Figure 8: Triple view of the central composition location. Azimuthal and radial plots (top) of composite wavenumbers  $\geq 2$  structures at the 10.5-km level, azimuthal cross section (left) and radial cross section (right) are shown. Positive vertical velocity (red contours) and positive vertical vorticity (blue contours) are displayed. Wind vectors composed of tangential and radial components (black arrows) are shown. Radar reflectivity values (with units of dBZ) are represented by shaded areas. The red asterisk denotes the central composition location.**

the 11-km level at 0 km radially and the 7.5-km level at -3km. The location of the positive vorticity inside of the updraft is consistent with the updraft tilting baroclinically-generated streamwise horizontal vorticity, convective stretching of pre-existing vertical vorticity from the hurricane environment, and the solenoidal effects produced by the local vertical wind shear. The intensity of the composited updraft can be witnessed by the associated wind vectors that show a persistent flow out of the eye/eyewall interface region at low levels, rising through the vortical updraft, and venting at upper levels.

Figure 9 represents an example of an azimuthal-radial plan view of the VHT composites depicting contours of perturbation vertical vorticity (cyclonic vorticity; blue contours), radar reflectivity (gray shading), and perturbation wind vectors (black arrows) for azimuthal wavenumbers greater than two. There

exist two vorticity features at the innermost radius of the composites at the 1.5-km level that are of particular importance. At the 3-km level (not shown), a local positive vertical vorticity maximum is present near  $-48^\circ$  and a negative vorticity feature is centered near  $+24^\circ$ . Within the cyclonic vorticity anomaly, a relatively weak updraft ( $> 1.0 \text{ m s}^{-1}$ ) is observed. The positive vorticity feature extends to about 6 km altitude. This relatively shallow vorticity feature collocated with anomalous vertical velocity is consistent with the definition of an eye-eyewall mesovortex (and will hereafter be referred to as a mesovortex). The mesovortex is also associated with enhanced outflow (presumably near the eye-eyewall interface). The wind vectors show air flowing from the inner vorticity feature and converging near  $0^\circ$  and 0 km. Convergence in this area is noteworthy because  $0^\circ$  and 0 km is the point of composition; therefore, it is possible that the strong VHT is being supplied with an appreciable amount of air from radii inside the eyewall.

To test whether the outflow observed in Fig. 9 is associated with convergence of low-level inflow from the environment (forced by the symmetric and wind shear circulations), a composite was constructed of the same vertical velocity and vorticity features associated

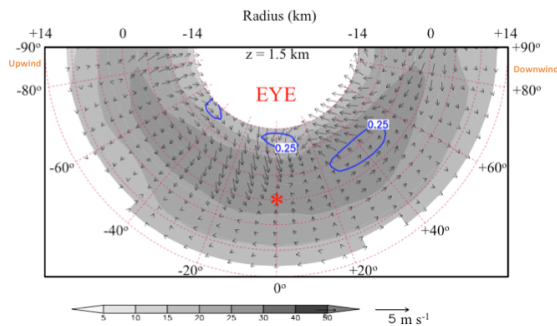


**Figure 9: Azimuthal and radial plan view plots of composite wavenumbers  $\geq 2$  structures at the 1.5-km level. Positive vertical vorticity (blue contours are displayed. Wind vectors composed of tangential and radial components (black arrows) are shown. Radar reflectivity values (with units of dBZ) are represented by shaded areas. The red asterisk denotes the central composition location.**

with wavenumbers zero and one (not shown). At 1.0 km, it is apparent that outflow and inflow are converging in the area between  $0^\circ$  and  $+20^\circ$  and along the line of 0 km radially, an area underneath the lower levels of the VHT. An examination of the 3-km level shows the outflow is dominant with the convergence area shifted cyclonically and radially outward. This flow pattern collocated radially and azimuthally demonstrates, at the very least, that convergence of inflow from outside of the eyewall and outflow from the lower eye is a common occurrence near VHTs.

## 6. SUMMARY

1. VHTs in Guillermo were defined as anomalously strong updrafts ( $w' \geq 5 \text{ m s}^{-1}$ ) that have a vertical depth  $\geq 6 \text{ km}$  that collocated with anomalously strong vorticity ( $+\zeta' \geq 1 \text{ m s}^{-1}$ ) through half of the depth of the updraft. An additional constraint that the  $w'$  maximum be at a higher altitude than the  $\zeta'$  maximum was also imposed. SEUs were defined as anomalously strong updrafts ( $w' \geq 5 \text{ m s}^{-1}$ ) with a vertical depth  $< 6 \text{ km}$ .
2. 16% of all XUPs satisfy the definition constructed for VHTs while 76% are SEUs.
3. XUPs represent  $\sim 10\%$  of all updrafts and occupy  $\sim 3\%$  of the updraft area, but transport  $\sim 15\%$  of all mass to upper levels of the troposphere.
4. VHTs are located primarily in the left-of-shear semicircle of the eyewall, while SEUs have no discernable azimuthal distribution pattern.
5. VHTs are confined to the eyewall, while SEUs are observed from the eye-eyewall interface to areas outside of the eyewall.
6. The bottoms (tops) of VHTs are 3.2 km lower (4.22 km higher) than SEUs. VHTs possess a mean depth of 9.75 km, while SEUs average 2.36 km. VHTs possess 225% stronger maximum median vertical velocities than SEUs ( $12.80 \text{ m s}^{-1}$  versus  $5.70 \text{ m s}^{-1}$ ). VHTs also exhibit a 6.6 km larger median diameter than SEUs (10.96 km versus 7.07 km).
7. VHTs transport 3.5 times more mass than SEUs while representing 5 times fewer extreme updrafts. VHTs also account for 2.6% of the updraft area but transport  $\sim 15\%$  of the mass. Additionally, VHTs contribute  $\sim 10\%$  more mass flux per unit area to the total mass flux than do SEUs.
8. Mesovortices are common low-level vorticity features located inward and upwind of VHTs. These mesovortices appear to contribute to air exchange across the eye-eyewall boundary. Convergence of low-level inflow from outside of the eyewall (mostly attributed to environmental vertical wind shear) and outflow from the lower eye (via mesovortices) is commonly located in close proximity to the lower levels of the typical VHT.

## REFERENCES

- Black, M.L., R.W. Burpee, and F.D. Marks, 1996: Vertical Motion Characteristics of Tropical Cyclones Determined with Airborne Doppler Radial Velocities. *J. Atmos. Sci.*, **53**, 1887–1909.

- Black, M.L., J.F. Gamache, F.D. Marks, C.E. Samsury, and H.E. Willoughby, 2002: Eastern Pacific Hurricanes Jimena of 1991 and Olivia of 1994: The Effect of Vertical Shear on Structure and Intensity. *Mon. Wea. Rev.*, **130**, 2291–2312.
- Eastin M. D., W. M. Gray, and P. G. Black, 2005b: Buoyancy of convective vertical motions in the inner core of intense hurricanes. Part II: Case Studies. *Mon. Wea. Rev.*, **133**, 209–227.
- Gamache, J. F., 1997: Evaluation of a fully three-dimensional variational Doppler analysis technique. Preprints, *28th Conf. on Radar Meteorology*, Austin, TX, Amer. Meteor. Soc.
- Gamache, J.F., F.D. Marks, and F. Roux, 1995: Comparison of Three Airborne Doppler Sampling Techniques with Airborne In Situ Wind Observations in Hurricane Gustav (1990). *J. Atmos. Oceanic Technol.*, **12**, 171–181.
- Hendricks, E.A., and M.T. Montgomery, 2006: Rapid Scan Views of Convectively Generated Mesovortices in Sheared Tropical Cyclone Gustav (2002). *Wea. Forecasting*, **21**, 1041–1050.
- Hendricks, E. A., M. T. Montgomery, and C. A. Davis, 2004: The role of “vortical” hot towers in the formation of tropical cyclone Diana (1984). *J. Atmos. Sci.*, **61**, 1209–1232.
- Heymsfield, G. M., J. B. Halverson, J. Simpson, L. Tian, and T. Paul Bui, 2001: ER-2 Doppler radar investigations of the eyewall of Hurricane Bonnie during the Convection and Moisture Experiment-3. *J. Appl. Meteor.*, **40**, 1310–1330.
- Hong, X., S. W. Chang, S. Raman, L. K. Shay, and R. Hodur, 2000: The interaction between Hurricane Opal (1995) and a warm core ring in the Gulf of Mexico. *Mon. Wea. Rev.*, **128**, 1347–1365.
- Houze, R.A., W.C. Lee, and M.M. Bell, 2009: Convective Contribution to the Genesis of Hurricane Ophelia (2005). *Mon. Wea. Rev.*, **137**, 2778–2800.
- Jorgensen, D.P., 1984: Mesoscale and Convective-Scale Characteristics of Mature Hurricanes. Part II. Inner Core Structure of Hurricane Allen (1980). *J. Atmos. Sci.*, **41**, 1287–1311.
- Julien, K., S. Legg, J. McWilliams, and J. Werne, 1996: Rapidly rotating turbulent Rayleigh–Benard convection. *J. Fluid Mech.*, **322**, 243–273.
- Kaplan, J., and M. DeMaria, 2003: Large-scale characteristics of rapidly intensifying tropical cyclones in the North Atlantic basin. *Wea. Forecasting*, **18**, 1093–1108.
- Kelley, O., and J. Stout, 2004: Convective towers in eyewalls of tropical cyclones observed by the TRMM precipitation radar in 1998–2001. Preprint, *20<sup>th</sup> Conference on Weather Analysis and Forecasting*, Seattle, Washington, Amer. Met. Soc.
- Malkus, J. S., C. Ronne, and M. Chaffee, 1961: Cloud pattern in Hurricane Daisy, 1958. *Tellus*, **13**, 8–30.
- Molinari, J., and D. Vollaro, 2008: Extreme Helicity and Intense Convective Towers in Hurricane Bonnie. *Mon. Wea. Rev.*, **136**, 4355–4372.
- Molinari J, Vollaro D (2009) Distribution of Helicity, CAPE, and Shear in Tropical Cyclones. *Journal of the Atmospheric Sciences*: In Press
- Montgomery, M. T., and R. J. Kallenbach, 1997: A theory for vortex Rossby waves and its application to spiral bands and intensity changes in hurricanes. *Quart. J. Roy. Meteor. Soc.*, **123**, 435–465.
- Montgomery, M. T., M. E. Nicholls, T. A. Cram, and A. B. Saunders, 2006: A vortical hot tower route to tropical cyclogenesis. *J. Atmos. Sci.*, **63**, 355–386.
- Reasor, P.D., M.T. Montgomery, and L.D. Grasso, 2004: A New Look at the Problem of Tropical Cyclones in Vertical Shear Flow: Vortex Resiliency. *J. Atmos. Sci.*, **61**, 3–22.
- Reasor, P.D., M.T. Montgomery, and L.F. Bosart, 2005: Mesoscale observations of the genesis of Hurricane Dolly (1996). *J. Atmos. Sci.*, **62**, 3151–3171.
- Reasor, P. D., and M. T. Montgomery, F. D. Marks Jr., and J. F. Gamache, 2000: Low-wavenumber structure and evolution of the hurricane inner core observed by airborne dual-Doppler radar. *Mon. Wea. Rev.*, **128**, 653–1680.
- Riehl, H., and J. S. Malkus, 1958: On the heat balance in the equatorial trough zone. *Geophysica*, **6**, 503–538.
- Rogers, R., 2009: Convective-Scale Structure and Evolution During a High-Resolution Simulation of Tropical Cyclone Rapid Intensification. *Journal of the Atmospheric Sciences*: In Press
- Shapiro L. J., and H. E. Willoughby, 1982: The response of balanced hurricanes to local sources of heat

and momentum. *J. Atmos. Sci.*, **39**, 378–394.

Shay, L. K., G. J. Goni, and P. G. Black, 2000: Effects of a warm oceanic feature on Hurricane Opal. *Mon. Wea. Rev.*, **128**, 1366–1383.

Simpson, J., J. B. Halverson, B. S. Ferrier, W. A. Petersen, R. H. Simpson, R. Blakeslee, and S. L. Durden, 1998: On the role of “hot towers” in tropical cyclone formation. *Meteor. Atmos. Phys.*, **67**, 15-35.

Sippel, J.A., J.W. Nielsen-Gammon, and S.E. Allen, 2006: The Multiple-Vortex Nature of Tropical Cyclogenesis. *Mon. Wea. Rev.*, **134**, 1796–1814.

Van Sang, N., R. K. Smith, and M. T. Montgomery, 2008: Tropical-cyclone intensification and predictability in three dimensions. *Quart. J. Roy Met. Soc.*, **134**, 563-582.

Willoughby, H., 1990: Temporal Changes of the Primary Circulation in Tropical Cyclones. *J. Atmos. Sci.*, **47**, 242–264.